Influence of manganese and nickel doping on optical and electric properties of CuO nanostructures for optoelectronic applications

Amna Bashir

Department of Chemistry,
Fatima Jinnah Women University,
The Mall, 46000, Rawalpindi, Pakistan
Email: amnabashir79@yahoo.com

Ambreen Naz

Department of Chemistry,
Quaid-i-Azam University Islamabad,
45320, Pakistan
Email: Ambreen_khan723@yahoo.com
Email: Ambreennaz72@gmail.com

Muhammad Sultan

Nanoscience and Technology Department,
National Centre for Physics,
45320, Islamabad, Pakistan
Email: mssatti79@yahoo.com

Rabia Bashir

School of Physics and Astronomy,
Yunnan University,
Kunming 650091, China
Email: rabia@mail.ynu.edu.cn

Naveed Zafar Ali

National Centre for Physics,
45320, Islamabad, Pakistan
Email: naveednik@gmail.com

Azhar Iqbal and Zareen Akhter*

Department of Chemistry,
Quaid-i-Azam University Islamabad,
45320, Pakistan
Email: aiqbal@qau.edu.pk
Email: zareenakhter@yahoo.com
*Corresponding author

Abstract: In recent years, metal oxide-based nanomaterials have gained considerable attention due to their wide range of applications in the field of catalysis, optoelectronics, and medicine. The current study is based upon the modification of optical and electronic properties of Cu(II) oxide (CuO) nanoparticles via doping. The CuO nanoparticles have been prepared by a simple hydrothermal route without using any template or surfactant. The optoelectronic modification of nanoparticles was done by the addition of dopants, i.e., 0%–5% nickel (Ni) and manganese (Mn). The powder X-rays diffraction (XRD) studies showed the improve crystallinitiy and increase particle size of CuO via doping. The field emission scanning electron microscopy (FE-SEM) showed the cauliflower and cluster-like nanostructures. The band-gap of Cu(II) oxide nanoparticles was investigated by the diffused reflectance spectroscopy (DRS). The photoluminescence (PL) measurements showed the increase in the surface defects and oxygen vacancies via the introduction of dopants. The presence of Ni and Mn in doped materials was confirmed by X-ray photoelectron spectroscopy (XPS). Hall measurements showed that the synthesised nanomaterials exhibit p-type conductivity. This modification of optoelectronic properties of CuO could present novel strategies leading to tailored metal oxide nanoparticles.

Keywords: copper oxides; metal oxides; optoelectronic properties; p-type; conductivity; CuO; p-type; doping; nanostructures; nanoflowers.

Reference to this paper should be made as follows: Bashir, A., Naz, A., Sultan, M., Bashir, R., Ali, N.Z., Iqbal, A. and Akhter, Z. (2022) 'Influence of manganese and nickel doping on optical and electric properties of CuO nanostructures for optoelectronic applications', *Int. J. Nanoparticles*, Vol. 14, No. 1, pp.13–30.

Biographical notes: Amna Bashir studied chemistry and received her Doctoral in Chemistry from the Quaid-i-Azam University Islamabad, Pakistan in 2018. She spent one year and six months as a research associate at Energy Research Institute at NTU, CREATE-SinBeRISE (Singapore-Berkeley Research Initiative for Sustainable Energy). She pursued her MS and MSc in Inorganic/Analytical Chemistry from the Quaid-i-Azam University Islamabad, Pakistan in 2012. She is currently working as an Assistant Professor at the Department of Chemistry, Fatima Jinnah Women University Rawalpindi, Pakistan. Her research focus on synthesis and doping of nanomaterials for advanced applications, such as photocatalysis and photovoltaic technologies with an emphasis on perovskite for a sustainable energy future.

Ambreen Naz has completed BSc in 2012 from Islamabad Model College for Girls, F7/2 Islamabad, Pakistan. She has done MSc and MPhil in Inorganic/Analytical Chemistry from the Quaid-i-Azam University Islamabad, Pakistan.

Muhammad Sultan has completed his PhD in the field of Ultrafast Dynamics of Nanostructures (Physics) from the Freie University Berlin in 2012. He is currently working as an Associate Professor at the Nanoscience and Technology Department of National Centre for Physics (NCP) Islamabad, where he is heading photovoltaics research group. His research interests include the engineered nanomaterials for solar energy harvesting, charge transfer and dynamics of solids, surfaces and interfaces, emerging nanomaterials and their applications.

Rabia Bashir studies at Yunnan University, Kunming China, since 2017 for her Doctoral in Applied Physics. She pursued her MS in Applied Physics from University of the Punjab Lahore, Pakistan. Her research focus on synthesis and doping of nanomaterials for advanced applications, such as energy storage devices and photovoltaic technologies with an emphasis colloidal quantum dots solar cells.

Naveed Zafar Ali is currently working as a Senior Scientist at National Centre for Physics, Quaid-I-Azam University Campus, Islamabad, Pakistan. He completed his PhD in the field of Solid State Physics from Max Planck Institute for Solid State Research, DE (2011). He pursued his postdoctorate study from Federal Institute for Materials Research and Testing: Berlin, DE (2017–2018). His research interest are homogeneous catalysis (energy, green and sustainable chemistry), upra-molecular chemistry (coordination chemistry and organometallics), and bio-inorganic chemistry.

Azhar Iqbal is currently working as an Associate Professor at Department of Chemistry, Quaid-i-Azam University Islamabad, Pakistan. He completed his PhD in 2010 from University of Warwick, UK. He pursued his postdoctorate study from Lund University, Sweden (2010–2013), and Nanyan Technological University, Singapore (2016–2018). His research interests include the femtosecond and picosecond studies of charge carriers dynamics using time-resolved fluorescence and transient absorption spectroscopies in semiconductor nanowires and quantum dots, mechanisms of charge/energy transfer processes in quantum-dot-sensitised solar cells and photochrome-fluorophore systems, synthesis and electro-optical characterisation of inorganic and organic semiconductors, with particular focus on photovoltaics, light emitting diodes and other energy devices, and photochemistry and photophysics of bio-molecules.

Zareen Akhter studied chemistry and received her Doctoral in Chemistry from the University of Cambridge, UK in 1996. She pursued her MS and MSc in Chemistry from the Quaid-i-Azam University Islamabad, Pakistan. She is currently working as a Professor at the Department of Chemistry, Quaid-i-Azam University Islamabad, Pakistan. She produced 57 MPhil and 12 PhD students up until now. Her research focus on synthesis and characterisation of ferrocene derivatives and ferrocene-based materials, transition metal complexes, and nanomaterials for advanced applications.

1 Introduction

Metal oxides semiconductors have a wide range of applications in the field of optoelectronics, gas sensing devices, and catalysis (Basith et al., 2014). The transition metals oxides nanomaterials (TMO) such as copper oxides (CuO), iron oxide (FeO),

nickel oxide (NiO), and zinc oxides (ZnO) possess unique physical and chemical properties due to their small size, high surface area, which is different from their bulk counterparts (Basith et al., 2014; Mageshwari et al., 2013). Amongst these TMO, the CuO attained considerable attention in recent years due to its narrow bandgap and favourable processing capabilities (Basith et al., 2014). The CuO nanomaterials are widely used in photocatalysis, gas sensors, adsorbent, supercapacitors, as an electrode of photocells, as well as in lithium-ion batteries (Basith et al., 2014; Dubal et al., 2013; Xu et al., 2011; Colmenares et al., 2006; Almquist and Biswas, 2002; Chen et al., 2004; Kiriakidou et al., 1999). Specifically in this class of materials, the mostly used form of CuO is copper (I) oxide (Cu_2O) (Pollack and Trivich, 1975; Tabuchi and Matsumura, 2002) and copper (II) oxide (CuO) (Chen et al., 2004; Tabuchi and Matsumura, 2002; Chiang et al., 2012; Masudy-Panah et al., 2016).

The CuO is a p-type semiconductor with good electric conductivity (Nandy et al., 2009), which arises from cationic vacancies present in the lattice that is generated during the preparation of nanoparticles (Chauhan et al., 2006; Kikuchi and Tonooka, 2005). The number of vacancies and hence conductivities vary depending upon the preparation methods. However, using these methods control over specific stoichiometry is quite challenging which leads to complication in final adjustment of the oxidation-reduction route (Kikuchi and Tonooka, 2005). Therefore, to improve the electric and optical properties of CuO the doping methods have been employed. The modification of optoelectronic properties of CuO is strongly dependent on the nature of the dopant employed (Ha et al., 2018). The variation in the optoelectronic properties of CuO nanoparticles via doping with Zn, Pb, Al, and Fe has been reported by various groups (Sonia et al., 2015; Bayansal et al., 2015; Basith et al., 2013). The other transition metals that have been reported include Ni, Ag, Li, and Bi (Basith et al., 2014; Bayansal et al., 2015; Chand et al., 2014; Huang et al., 2012; Dagdelen et al., 2012). The CuO nanoparticles doped with Ni ions exhibit hexagonal crystal structure and show ferromagnetic behaviour at room temperature (Basith et al., 2014). Similarly, Mn-doped CuO nanoparticles have been reported by Rao et al. (2007). They reported that the coexistence of Mn^{+2} and Mn^{+3} ions and the binary exchange mechanism are responsible for the ferromagnetism in Mn-doped CuO nanoparticles. Jiang et al. (2016) report the optical and photocatalytic properties of CuO affected by Mn doping. The chain mechanism was developed by Zhao et al. (2008) to explain the ferromagnetism in Mn-doped CuO nanoparticles. Furthermore, the CuO nanoparticles doped with Mn, Fe, Co, and co-doped with neodymium (Nd) have also been reported in Basith et al. (2014), Bayansal et al. (2015), Chand et al. (2014), Huang et al. (2012) and Dagdelen et al. (2012).

The present study is conducted to modify the optoelectronic properties of CuO nanoparticles for future applications. With this motivation, the Ni (1%–5%) and Mn (1%–5%) doped CuO nanoparticles were synthesised by the hydrothermal method. The optical properties were investigated by photoluminescence (PL) and ultraviolet-visible spectroscopy (UV-Vis). The electrical properties were examined using four-probe and hall measurements. The crystal structure, morphology, and stoichiometry of nanoparticles were explored using X-ray diffraction (XRD), scanning electron microscopy (SEM), and X-ray photoelectron spectroscopy (XPS), respectively.

2 Materials and methods

2.1 Synthesis of pure and doped CuO nanoparticles

The CuO nanoparticles were synthesised by using modified hydrothermal methods (Wang et al., 2015). The precursor solutions were prepared by dissolving metal salts in distilled water. Briefly, the solution was prepared by mixing 50 mL of 0.1 M NaOH and 40 mL of 0.4 M $Cu(CH_3COO)_2$ with constant agitation. The doping was done by adding a suitable amount of $NiCl_2.6H_2O$, (in the case of Ni-doped CuO), and ($MnCl_2.6H_2O$ in the case of Mn-doped CuO) to the above solution. The hydrothermal treatment was done by transferring the above solution in the autoclave having Teflon lining. The suspension was heated in an oven at 5°C per minute at 110°C for 2 hours. After 2 hours the black product was separated by centrifugation and washed many times using de-ionised water and ethanol. The synthesised CuO nanoparticles were then dried at 90°C for 12 hours in a vacuum oven (Wang et al., 2015). The schematic representation of the synthesis of CuO nanoparticles is shown in Figure 1.

Figure 1 Schematic representation of the synthesis of CuO nanoparticles (see online version for colours)

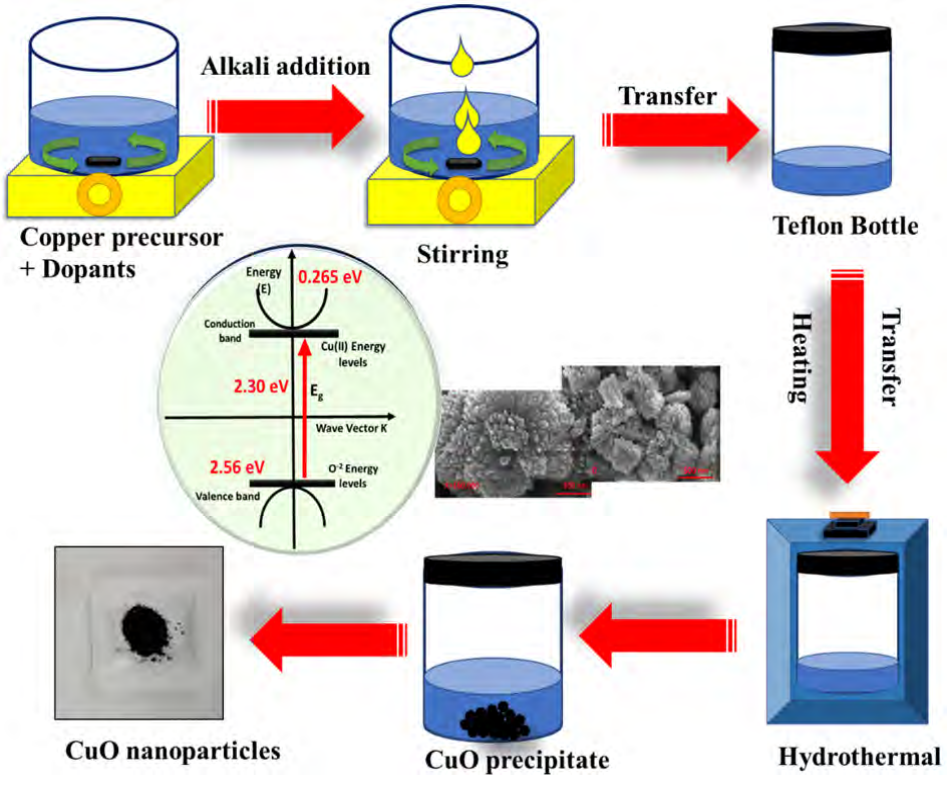

The flame atomic absorption spectrophotometric (FAAS) studies were used to find percent contents of doped elements (Perkin Elmer Analyst 400) (Balcerzak, 2002). The powder XRD was done using 3040/60-X-Pert Pro having Cu Kα1 as a radiation source. The morphological studies of prepared nanoparticles were done using FE-SEM, TESCAN, Czech Republic. The prepared nanomaterials were further characterised by the and UV-Vis diffused reflectance spectrophotometer (Perkin Elmer Lambda 35). XPS measurements were performed under high vacuum conditions using Omicron system. The monochromatised Al Kα X-ray source (1,486.7 eV) with Argus hemispherical electron spectrometer with 128 channels MCP detectors was used. For the PL decay measurements, the excitation of the sample was made at 306 nm with a pulsed LED excitation source coupled to FT-300 spectrometer, PicoQuant, Germany. The instrument works on the principle of the time-correlated single-photon counting (TCSPC) technique. The hall measurements were conducted using Keithley source metre (2,450) by applying the magnetic field of 0.58 T perpendicularly to the sample plane.

3 Results and discussion

3.1 Structural characterisation

Figure 2(a) demonstrated the XRD pattern of as-prepared CuO nanoparticles with and without Ni doping. The pronounced peaks at 2θ values of 32.15, 35.55, 38.73, 48.76, 53.41, 61.57, 66.22, 68.14, 72.41, and 75.02 are corresponding to the (110), (–111), (111), (–202), (202), (–113), (113), (220), and (311) planes, respectively (Khan et al., 2013). The presence of these diffraction peaks and their sharpness confirmed the formation of the single monoclinic phase of CuO nanoparticles (*JCPDS card No. 05-0661*) (Khan et al., 2013; Iqbal et al., 2017). Furthermore, the absence of diffraction patterns of Ni, NiO, and Cu_2O confirms the phase purity of synthesised nanomaterials. In the case of Ni-doped CuO, the peak position remains almost the same as that of pure CuO nanoparticles. This is because of the approximately same sizes of Cu^{+2} (0.73 Å) and Ni^{+2} (0.69 Å) ions, and exchange of these ions results in the no observable distortion in the lattice parameter of CuO (Meneses et al., 2008). The crystal structure of CuO nanoparticles is shown in Figure 2(b).

The Debye-Scherrer equation (Marczenko et al., 1980; Bashir et al., 2019; Bashir et al., 2020a, 2020b) is used to check the variation of crystallite size of nanomaterial with the dpoing (Titirici et al., 2006; Williamson and Smallman, 1956; Prabu et al., 2017; Shkir and AlFaify, 2017). The results are presented in Table 1. The results showed the increase in the crystallite size from 20 to 54 nm after the introduction of Ni as a dopant. This increase in the crystallite size might be due to the:

1 distortion in the crystal lattice of CuO after doing with the Ni ion

2 prevention of the direct contact between the particles due to the movement of Ni ion at boundaries of grains

3 or due to the smaller ionic radii of Ni^{+2} (0.69 Å) as compared to Cu^{+2} (0.73 Å) (Shkir and AlFaify, 2017).

With the help of the XRD pattern, various other structural parameters were also calculated and listed in Table 1.

Figure 2 (a) XRD pattern un-doped and doped nanomaterial, (b) A representation typical crystal structure of pure CuO nanoparticle (see online version for colours)

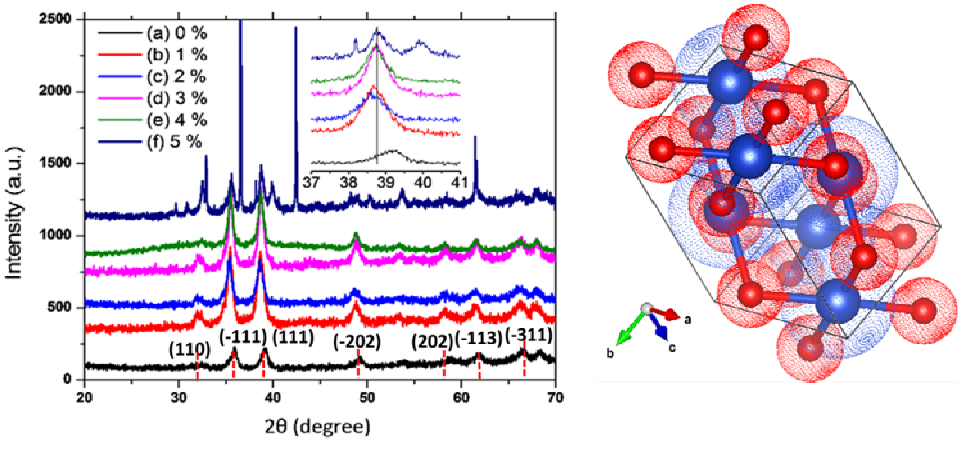

(a) (b)

Table 1 Crystallite size, lattice parameters, cell volume of synthesised nanoparticles

Sample	*Lattice parameters*				*Cell volume*	*Weight % of Ni*
	Crystallite size (nm)	*a(Å)*	*b(Å)*	*c(Å)*		
CuO	20.0	4.68	3.44	5.13	81.90	0
Ni-1%	23.0	4.68	3.44	5.13	81.88	1.02
Ni-2%	27.2	4.68	3.44	5.13	81.56	2.22
Ni-3%	31.5	4.68	3.43	5.13	81.41	2.98
Ni-4%	39.8	4.68	3.43	5.13	81.30	4.00
Ni-5%	42.2	4.68	3.43	5.13	81.22	5.15

Figures 3(a) and 3(b) demonstrate the diffraction results of synthesised CuO and without and with Mn doping. The diffraction pattern is matching well with the JCPDS card number *01-080-0076*, corresponding to the monoclinic phase of CuO (Iqbal et al., 2017). Furthermore, the sharpness of the peaks depicted the highly crystalline nature of CuO with and without doping. In the CuO system, a slight distortion in the crystal structure is observed due to the substitution of Cu^{+2} by Mn^{+2} ions as seen from shifting of the diffraction peak at θ = 35.45° and 38.85° [Figure 3 (b)]. The shifting of peaks is already reported in the literature which might be due to the formation of defects and oxygen vacancies (Ha et al., 2018). The stronger peaks present at θ = 35.45° and 38.85° showed the preferred crystal planes of nanoparticles. No other peak related to impurities such as Mn or hydroxide is observed in the diffraction pattern. It is observed that peak intensity is increased with Mn doping and is maximum for the 5% Mn-doped CuO nanoparticles.

Table 2 showed the crystallite size of CuO nanoparticles with and without Mn doping. The crystallite sizes range from 23.7 nm to 20.0 nm. Lattice distortion has been induced by Mn doping and, resultant an increase in the crystallite size and lattice parameters is observed. Due to greater ionic radii of Mn^{+2} (0.83 Å) as compared to Cu^{+2} (0.73 Å) the increase in crystallite size and ionic radii has been observed as already

reported in Chandramohan et al. (2018). The other parameters such as cell volume and unit cell lengths of synthesised nanoparticles are shown in Table 2.

Figure 3 XRD pattern of Mn-doped CuO nanoparticles (b) Enlarged view of the peak at 38.85 and 35.55, variation of cell volume and particle size with metal contents (c) For the Ni doped CuO (d) For Mn-doped CuO (see online version for colours)

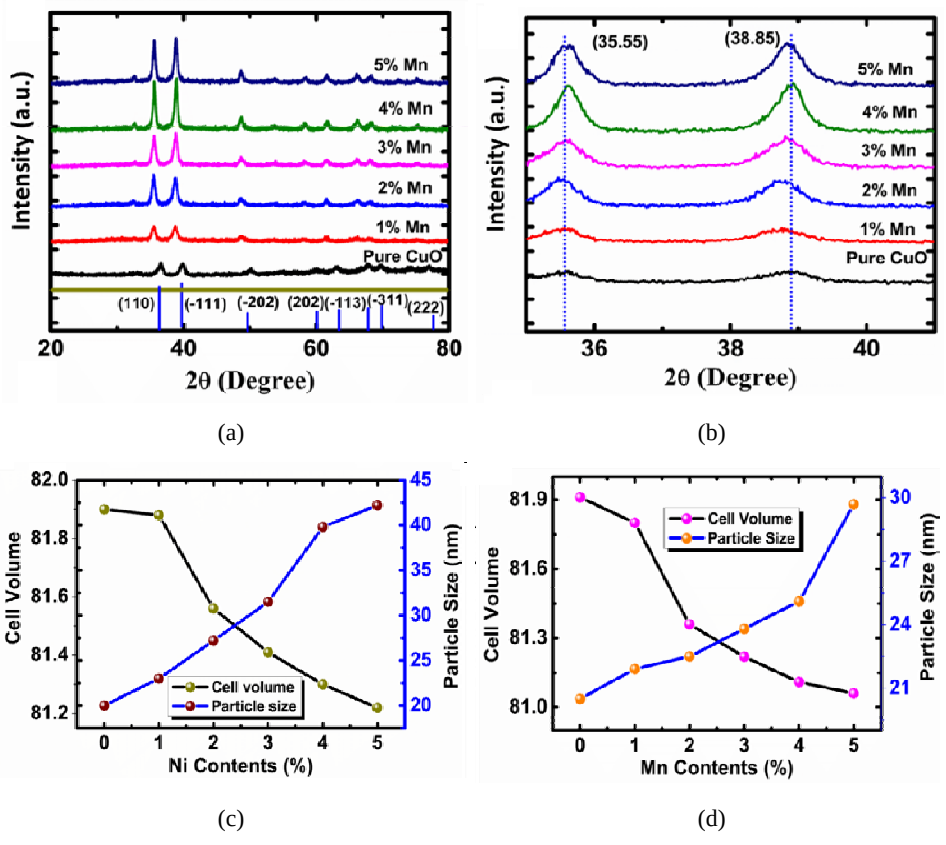

(a) (b)

(c) (d)

Table 2 Crystallite size, lattice parameters, cell volume of synthesised nanoparticles

Sample	*Lattice parameters*				*Cell volume*	*Weight % of Mn*
	Crystallite size (nm)	*a(Å)*	*b(Å)*	*c(Å)*		
CuO	20.5	4.68	3.43	5.13	81.91	0
Mn-1%	21.9	4.68	3.42	5.14	81.80	1.23
Mn-2%	22.5	4.68	3.42	5.14	81.36	1.82
Mn-3%	23.8	4.68	3.42	5.15	81.22	2.87
Mn-4%	25.1	4.68	3.43	5.15	80.11	3.90
Mn-5%	29.7	4.68	3.43	5.15	80.06	5.00

The lattice parameters obtained from the XRD pattern for Ni and Mn doped CuO nanoparticles are shown in Tables 1 and 2. No systematic trend is observed for the variation in the unit cell lengths of doped and un-doped nanoparticles. It might be due to

the complexity of the monoclinic crystal structure of CuO and anisotropic variation in the crystal lattice. The variation of unit cell volume and crystallite size obtained from the XRD pattern as a function of dopant concentration is shown in Figures 3(c) and 3(d). From the figure, it is clear that unit cell volume and crystallite size vary with the dopant concentration, thus confirming the incorporation of Ni and Mn ions within the CuO host lattice.

The presence of dopants and oxidation states of metals in synthesised nanostructures is confirmed by the XPS. The XPS spectrum of Ni-doped CuO (5% Ni) is shown in Figures 4(a) and 4(c). The peaks for Cu, O, and Ni are observed, which confirms the presence of dopants in the sample. The magnified XPS spectra for $Cu2p_{3/2}$ and $Cu2p_{1/2}$ are shown in Figure 4(a). The peak at 936.08 eV is corresponding to the $Cu2p_{3/2}$ which confirms the growth of CuO nanostructures. XPS spectrum shows the presence of two strong satellite peaks. These peaks are characteristics peaks of Cu^{+2}. It is possible to distinguish between different oxidation states of Cu using these satellite features. The $Cu2p_{3/2}$ peak in Cu (II) is shifted and is much wider as compared to Cu (I) oxide. Thus the XPS spectra confirm that copper is present only in Cu^{+2} state (Ha et al., 2018).

Figure 4(b) shows the XPS spectra of O1s. The broad and asymmetric peaks indicate that there is more than one chemical form of oxygen existing in the sample. Two main oxygen peaks are observed in the spectra. The peak at 528.96 eV is corresponding to the lattice oxygen (Cu-O bond), and it makes the primary contribution to the spectrum. The other peak that appeared at 532.88 eV is corresponding to the chemisorbed surface hydroxyl oxygen (O-H bond) (Ha et al., 2018). Figure 4(c) showed the XPS spectrum of $Ni2p_{3/2}$ and $Ni2p_{1/2}$. The peak at 855.56 eV is corresponding to the $Ni2p_{3/2}$ level, while the peak at 851.81 eV is assigned to the $Ni2p_{1/2}$. These satellite peaks for $Ni2p_{3/2}$ and $Ni2p_{1/2}$ confirmed the formation of NiO nanostructures (Ha et al., 2018).

The XPS septum of CuO doped with Mn^{+2} is demonstrated in Figures 4(d) and 4(f). Again, the peak appeared at 936.08 eV with two satellites corresponding to $Cu2P_{3/2}$ confirm the presence of Cu^{+2} ions in the sample [Figure 4(d)]. The XPS spectrum for O1s is shown in Figure 4(e). The two peaks were observed, i.e., at 529.08 eV and 533.26 eV, corresponding to the Cu-O bond and surface adsorbed OH groups. The XPS spectra of Mn2P are shown in Figure 4(f). The two peaks appeared at 644.21 eV and 651.98 eV. These two peaks are corresponding to the Mn^{+2} ions. The absence of the peak at 638.7 eV and 641.4 eV confirmed the absence of Mn metal and MnO_2 in the synthesised nanostructures. So, in synthesised nanomaterials, the Mn is present in a +2 oxidation state.

3.2 Morphological studies

The exact percentage of Ni and Mn in the doped CuO sample is measured using FAAS as presented in Tables 1 and 2. The values obtained are well matching with the proposed results. The SEM images of pure CuO nanoparticles are shown in Figures 5(a) and 5(d). It is clear from images that pure CuO exhibited flower-like morphology. This cauliflower-like morphology was also observed by Dubal et al. and Jianjian Shi et al. (Zhao et al., 2008). The undoped CuO nanoparticles have aggregated together leading to a bigger grain size similar to the cluster or flower-like appearance.

Figure 4 The XPS spectrum of CuO with Ni^{+2} doping, (a) Cu2P, (b) O1s, (c) Ni 2P, XPS spectrum of Mn^{+2} doped CuO, (c) $Cu2P_{3/2}$, (d) O1s, (e) Mn $2P_{3/2}$ (see online version for colours)

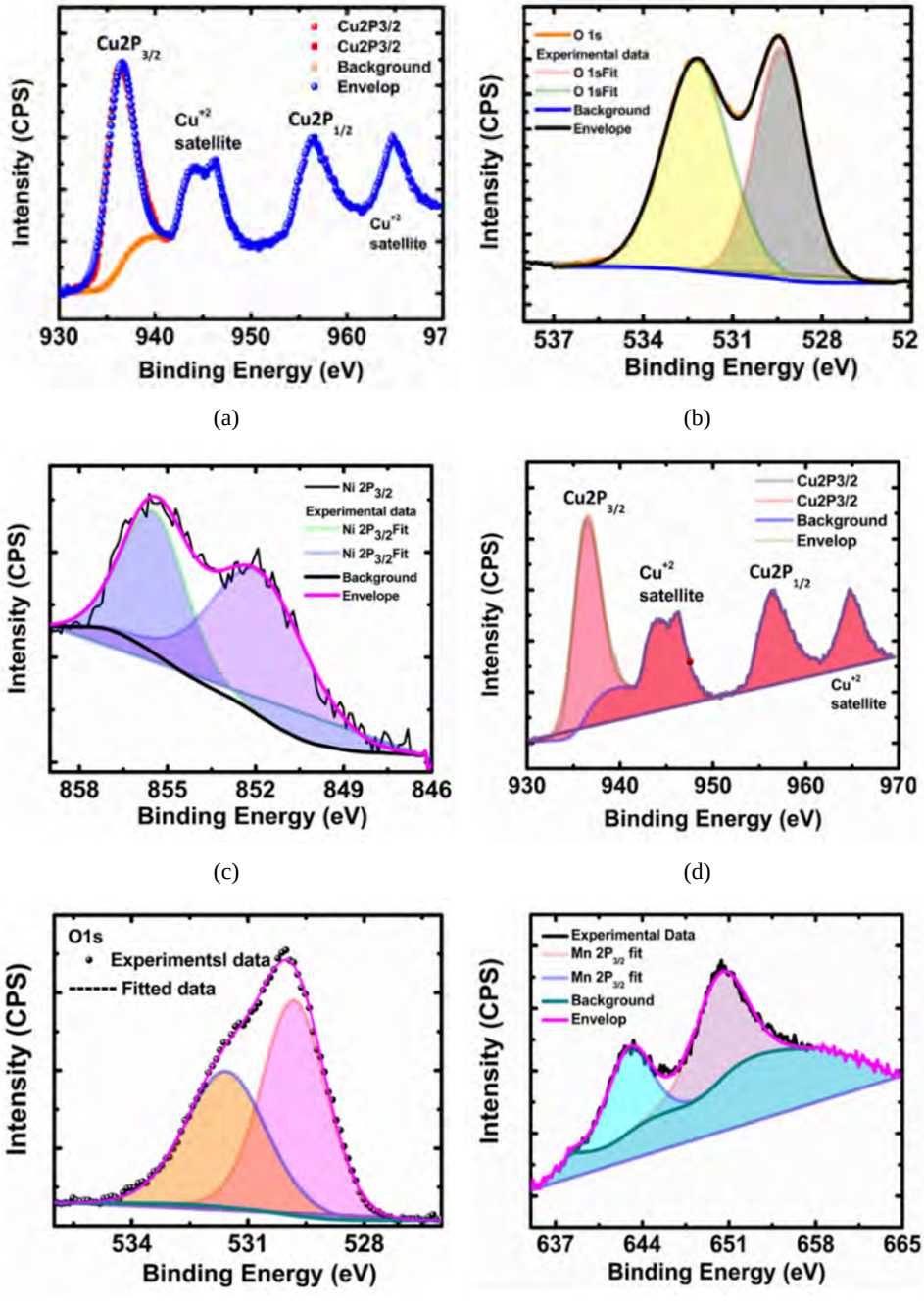

Figure 5 SEM images of pure CuO nanoparticles, (a) X = 20,000 (b) X = 40,000 (c) X = 80,000 (d) 160,000 (see online version for colours)

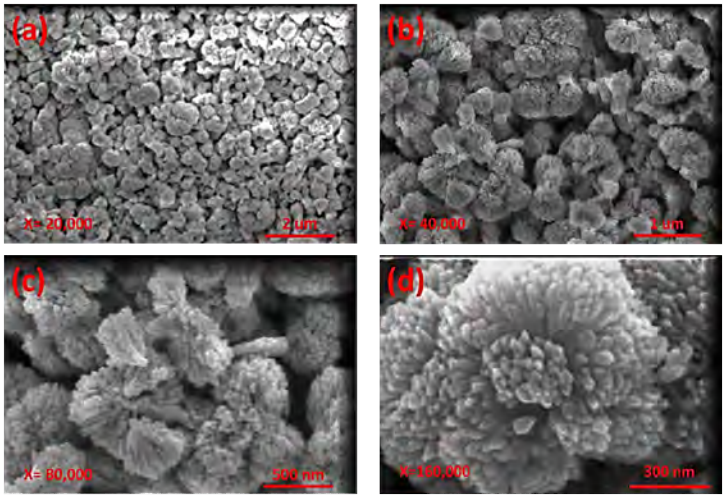

The SEM images of CuO nanoparticles doped with various concentration of Ni are shown in Figures 6(a) and 6(c). With the increase in Ni concentration, the grain size also increased as clear from figure. However, the flower-like appearance of nanoparticles decreased with Ni concentration and that is because of the doping effect of Ni^{+2} ions in the crystal lattice of CuO. With 5% Ni contents the morphology appeared like collapsed clusters (Basith et al., 2014; Dubal et al., 2013).

Figure 6 SEM images of Ni doped CuO nanoparticles, (a) 1% Ni (b) 3% Ni (c) 5% Ni (see online version for colours)

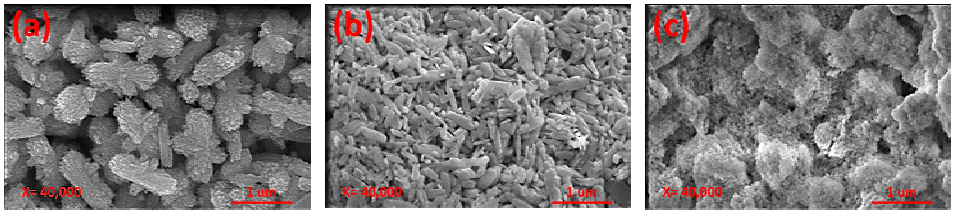

The SEM images for Mn-doped CuO nanoparticles are shown in Figures 7(a) and 7(f). The results are similar as obtained for CuO doped with Ni^{+2} ions. The increase in grain size is observed for various concentrations of Mn. However, the morphology changed from a flower-like appearance to collapsed clusters. The presence of Mn^{+2} ions at interstitial points in CuO lattice is the main reason for the change in the morphology of nanoparticles with doping (Dubal et al., 2013).

3.3 Optical properties

The variation in the optical properties of CuO via doping is analysed by DRS. The data was recorded in the range of 200–1,100 nm. The absorption spectrum of CuO with and without Ni^{+2}/Mn^{+2} ions is presented in Figures 8(a) and 8(b). In the case of Ni/Mn-doped

CuO the absorption intensity increased with the doping concentration. The optical band gap energies were calculated by using relationship $(\alpha\ h\nu) = A(h\nu - Eg)^n$ (Callister and Rethwisch, 2011). In the case of Ni-doped CuO blue shift is observed in absorption spectra of the synthesised nanoparticles. The calculated band gap energy for pure CuO nanoparticles is equal to 1.26 eV. However, the band gap for doped CuO increased to 1.31 eV, 1.34 eV, 1.36 eV for 1%, 3% and 5% Ni doping, respectively [Figure 8(c)].

Figure 7 SEM images of Mn doped CuO, (a)–(b) 1% Mn (c)–(d) 3% Mn (e)–(f) 5% Mn (see online version for colours)

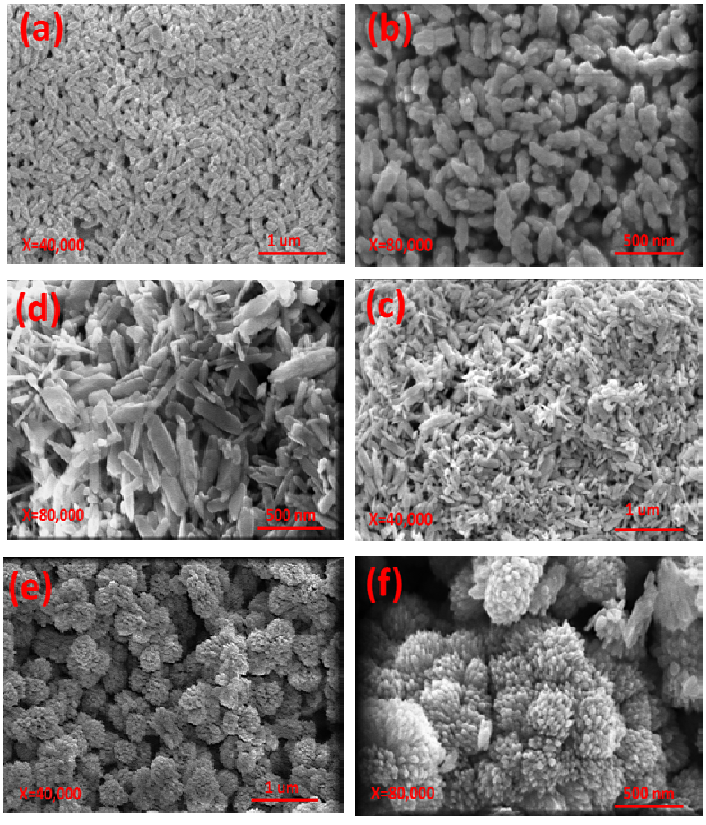

In the case of Mn-doped nanoparticles, the absorption edge is shifted towards the lower wavelength. The calculated bandgap is 1.76 eV, 1.70 eV, 1.65 eV and 1.60 eV for pure, 1% Mn, 3% Mn and 5% Mn-doped nanoparticles, respectively [Figure 8(c)]. The increased bandgap observed in this case can be attributed to a well-known effect that is band tailing effect (Basith et al., 2014; Chand et al., 2014; Jayaprakash et al., 2015). The calculated band-gap energies for CuO nanoparticles doped with Mn^{+2} are greater than the pure CuO. This increase in band-gap is further supported by literature values (Basith et al., 2014; Jayaprakash et al., 2015).

The PL is a very useful tool to determine band-gap energy and to check the purity of nanomaterials as, semiconductor oxide's emission is affected by many factors s, including the morphology of particle, concentration, and size of dopant. The representative PL plots of CuO with and without (3%) Mn^{+2}/Ni^{+2} ions are represented in

Figure 8(d). The representative sample showed green colour emission peaks at 530 nm in the visible region of the spectrum. This PL peak is not due to the band-gap emission but can be attributed to the defects and oxygen vacancies present in the synthesised nanoparticles (Ramya et al., 2016). These defects sites and oxygen vacancies increase with the doping. These generally act as intrinsic defects and results in the generation of a new energy gap between the valance and conduction gap of CuO nanostructures. It is clear from the graphs that PL intensity [Figure 8(d)] is gradually increased from pure CuO to Mn and Ni-doped CuO, corresponding to the increased surface defects, oxygen vacancies, and more availability of photogenerated charge carriers in the prepared materials (Basith et al., 2014; Kannaki et al., 2016).

Figure 8 (a) UV-Vis of CuO with and without Ni^{+2} ions (b) UV-Vis of CuO with and without Mn^{+2} ions (c) Variation of bandgap in case of Ni/Mn-doped CuO (d) PL spectrum of representative samples (see online version for colours)

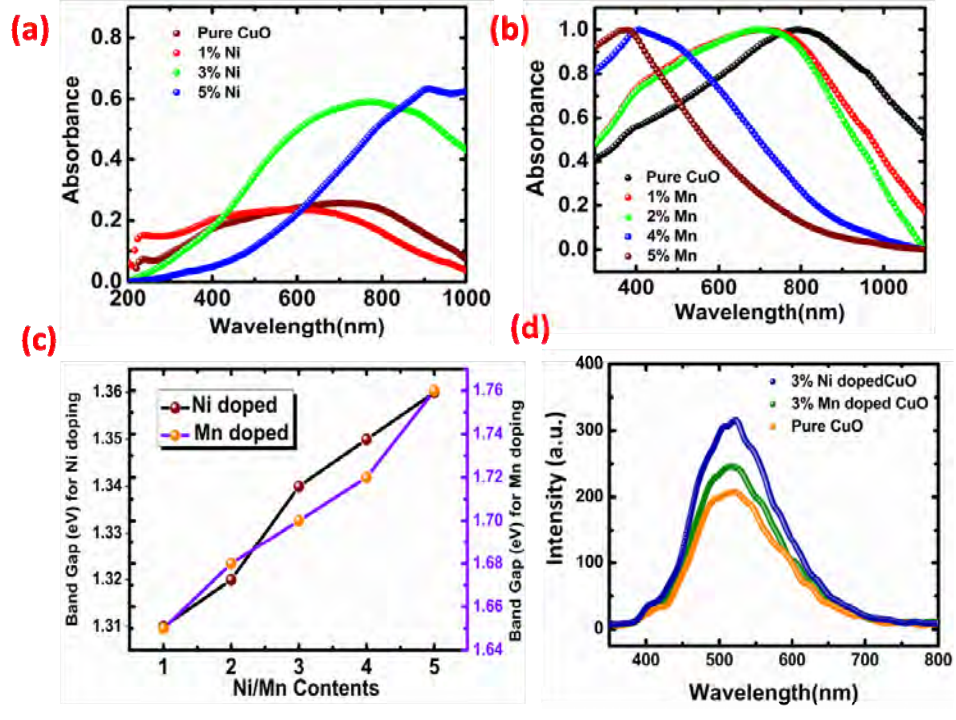

3.4 Electrical properties

The electric properties of pure and doped CuO nanostructures are accessed using Hall measurements. The measurement is done using the Vander Pauw configuration at room temperature. The data showed that the Hall coefficient is greater than zero for pure and doped samples, which indicates that all samples exhibited p-type conductivity. The resistivity for various samples is demonstrated in Table 3. The data showed that the values of electric resistivity vary slightly with the various concentration of Ni and Mn. In general, the value of resistivity decreased with the introduction of dopant. The increase in conductivity is due to the increase in the surface defects and Cu vacancies with the

dopant concentration. As already reported in the literature that the increase in electric conductivity of CuO film is due to the development of more Cu vacancies (Ogwu et al., 2007; Drobny and Pulfrey, 1979).

Table 3 Variation of resistivity of CuO with Ni/Mn doping

Sample	*Resistivity (Ohm cm)*	*Sample*	*Resistivity (Ohm cm)*
CuO	1.93E4	CuO	1.88E4
Ni-1%	1.67E3	Mn-1%	1.78E3
Ni-3%	1.26E2	Mn-3%	1.47E2
Ni-5%	1.18E2	Mn-5%	1.20E2

The variation of carrier concentration and mobility with various concentrations of Mn/Ni is shown in Figures 9(a) and 9(b). From Figure 9 it is clear that the carrier concentration and carrier mobility increase with doping in both cases. In the case of Ni doping the carrier, concentration is increased from 1E15 to 4E15 per cm^3. However, the mobility increased from 10 to 23 $cm^2V^{-1}S^{-1}$. Similar results have been obtained in the case of Mn-doped CuO nanoparticles [Figure 9(a)]. One possible reason for the increase in carrier concentration in both cases is due to the increase in the Cu vacancies with doping. The improvement in the mobility might be due to the improved crystallinity of CuO nanostructures with Ni and Mn doping as already reported in Gopalakrishna et al. (2013), Jundale et al. (2012), Gonçalves et al. (2009) and Shen et al. (2015).

Figure 9 Carrier concentration and carrier mobility in case of (a) pure and Ni doped samples and (b) pure and Mn doped samples (see online version for colours)

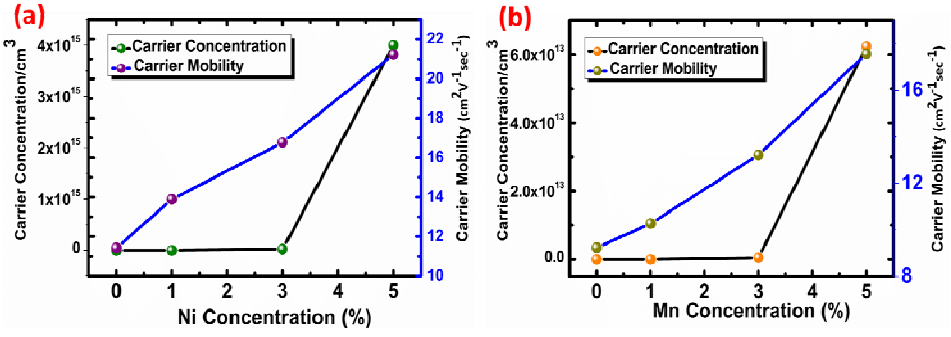

4 Conclusions

The hydrothermal method was used to synthesise CuO nanoparticles and it was proved to be a successful way of obtaining pure and doped nanoparticles. These nanoparticles were characterised by different techniques such as XRD, UV-Vise and PL, XPS, and SEM analysis. Newly synthesised nanoparticles have larger surface areas and their light absorption ability has been extended to the visible region which can enhance their photocatalytic activity as depicted through PL and UV-Vis spectroscopic studies. Cupric oxide has gained importance because of its usage in optoelectronics and electronic devices, gas sensors, nanofluids, high-temperature superconductors, magnetic storage

devices, and catalysts. It is expected that the nanoparticles being synthesised may offer some exciting opportunities for potential applications in solar cells, catalysis, and high-temperature superconductors.

Acknowledgements

We are thankful to Quaid-i-Azam University and the National Center for Physics Islamabad for access to the characterisations techniques.

References

Almquist, C.B. and Biswas, P. (2002) 'Role of synthesis method and particle size of nanostructured TiO2 on its photoactivity', *Journal of Catalysis*, Vol. 212, No. 2, pp.145–156.

Balcerzak, M. (2002) 'Sample digestion methods for the determination of traces of precious metals by spectrometric techniques', *Analytical Sciences*, Vol. 18, No. 7, pp.737–750.

Bashir, A., Bashir, F., Mehmood, Z., Satti, M.S. and Akhter, Z. (2019) 'Synthesis, characterisation and investigation of enhanced photocatalytic activity of Sm+ 3, Ni+ 2 co-doped TiO2 nanoparticles on the degradation of azo dyes in visible region', *International Journal of Nanoparticles*, Vol. 11, No. 1, pp.37–61.

Bashir, A., Bashir, F., Sultan, M., Mubeen, M., Iqbal, A. and Akhter, Z. (2020a) 'Influence of nickel and lanthanum ions co-doping on photocatalytic properties of TiO2 for effective degradation of reactive yellow 145 in the visible region', *Journal of Sol-Gel Science and Technology*, Vol. 93, No. 2, pp.438–451.

Bashir, A., Bashir, F. and Akhter, Z. (2020b) 'Preparation and performance analysis of γ-Al2O3 supported Cu-Ru bimetallic catalysts for the selective wet air oxidation of aqueous ammonia to nitrogen', *Journal of Nanostructures*, Vol. 10, No. 1, pp.28–38.

Basith, N.M., Vijaya, J.J., Kennedy, L.J. and Bououdina, M. (2013) 'Structural, optical and room-temperature ferromagnetic properties of Fe-doped CuO nanostructures', *Physica E: Low-Dimensional Systems and Nanostructures*, Vol. 53, pp.193–199.

Basith, N.M., Vijaya, J.J., Kennedy, L.J. and Bououdina, M. (2014) 'Structural, morphological, optical, and magnetic properties of Ni-doped CuO nanostructures prepared by a rapid microwave combustion method', *Materials Science in Semiconductor Processing*, Vol. 17, pp.110–118.

Bayansal, F., Gülen, Y., Şahin, B., Kahraman, S. and Çetinkara, H. (2015) 'CuO nanostructures grown by the SILAR method: influence of Pb-doping on the morphological, structural and optical properties', *Journal of Alloys and Compounds*, Vol. 619, pp.378–382.

Callister, W.D. and Rethwisch, D.G. (2011) *Materials Science and Engineering*, Vol. 5, John Wiley & Sons, NY.

Chand, P., Gaur, A., Kumar, A. and Gaur, U.K. (2014) 'Structural and optical study of Li doped CuO thin films on Si (1 0 0) substrate deposited by pulsed laser deposition', *Applied Surface Science*, Vol. 307, pp.280–286.

Chandramohan, R., Valanarasu, S., Ganesh, V., Shkir, M., Kathalingam, A. and AlFaify, S. (2018) 'Facile synthesis and characterization of undoped, Mn doped and Nd co-doped CuO nanoparticles for optoelectronic and magnetic applications', *Journal of Molecular Structure*, Vol. 1171, pp.388–395.

Chauhan, D., Satsangi, V., Dass, S. and Shrivastav, R. (2006) 'Preparation and characterization of nanostructured CuO thin films for photoelectrochemical splitting of water', *Bulletin of Materials Science*, Vol. 29, No. 7, pp.388–395.

Chen, Y., Wang, K. and Lou, L. (2004) 'Photodegradation of dye pollutants on silica gel supported TiO2 particles under visible light irradiation', *Journal of Photochemistry and Photobiology A: Chemistry*, Vol. 163, Nos. 1–2, pp.281–287.

Chiang, C-Y., Shin, Y., Aroh, K. and Ehrman, S. (2012) 'Copper oxide photocathodes prepared by a solution based process', *International Journal of Hydrogen Energy*, Vol. 37, No. 10, pp.8232–8239.

Colmenares, J., Aramendia, M., Marinas, A., Marinas, J. and Urbano, F. (2006) 'Synthesis, characterization and photocatalytic activity of different metal-doped titania systems', *Applied Catalysis A: General*, Vol. 306, pp.120–127.

Dagdelen, F., Serbetci, Z., Gupta, R. and Yakuphanoglu, F. (2012) 'Preparation of nanostructured Bi-doped CdO thin films by sol–gel spin coating method', *Materials Letters*, Vol. 80, pp.127–130.

Drobny, V. and Pulfrey, L. (1979) 'Properties of reactively-sputtered copper oxide thin films', *Thin Solid Films*, Vol. 61, No. 1, pp.89–98.

Dubal, D.P., Gund, G.S., Lokhande, C.D. and Holze, R. (2013) 'CuO cauliflowers for supercapacitor application: novel potentiodynamic deposition', *Materials Research Bulletin*, Vol. 48, No. 2, pp.923–928.

Gonçalves, A., Campos, L., Ferlauto, A. and Lacerda, R. (2009) 'On the growth and electrical characterization of CuO nanowires by thermal oxidation', *Journal of Applied Physics*, Vol. 106, No. 3, p.034303.

Gopalakrishna, D., Vijayalakshmi, K. and Ravidhas, C. (2013) 'Effect of annealing on the properties of nanostructured CuO thin films for enhanced ethanol sensitivity', *Ceramics International*, Vol. 39, No. 7, pp.7685–7691.

Ha, J-w., Oh, J., Choi, H., Ryu, H., Lee, W-J. and Bae, J-S. (2018) 'Photoelectrochemical properties of Ni-doped CuO nanorods grown using the modified chemical bath deposition method', *Journal of Industrial and Engineering Chemistry*, Vol. 58, pp.38–44.

Huang, J., Wu, H., Cao, D. and Wang, G. (2012) 'Influence of Ag doped CuO nanosheet arrays on electrochemical behaviors for supercapacitors', *Electrochimica Acta*, Vol. 75, pp.208–212.

Iqbal, M., Sial, M.A.Z.G., Shabbir, S., Siddiq, M. and Iqbal, A. (2017) 'Effect of Fe doping on the crystallinity of CuO nanotubes and the efficiency of the hybrid solar cells', *Journal of Photochemistry and Photobiology A: Chemistry*, Vol. 335, pp.112–118.

Jayaprakash, J., Srinivasan, N., Chandrasekaran, P. and Girija, E. (2015) 'Synthesis and characterization of cluster of grapes like pure and zinc-doped CuO nanoparticles by sol–gel method', *Spectrochimica Acta Part A: Molecular and Biomolecular Spectroscopy*, Vol. 136, pp.1803–1806.

Jiang, T., Kong, J., Wang, Y., Meng, D., Wang, D. and Yu, M. (2016) 'Optical and photocatalytic properties of Mn-doped CuO nanosheets prepared by hydrothermal method', *Crystal Research and Technology*, Vol. 51, No. 1, pp.58–64.

Jundale, D., Joshi, P., Sen, S. and Patil, V. (2012) 'Nanocrystalline CuO thin films: synthesis, microstructural and optoelectronic properties', *Journal of Materials Science: Materials in Electronics*, Vol. 23, No. 8, pp.1492–1499.

Kannaki, K., Ramesh, P.S. and Geetha, D. (2016) 'Facile hydrothermal synthesis and structural, optical, and morphological investigations on PVP assisted Fe doped CuO nanocomposites', *Materials Today: Proceedings*, Vol. 3, No. 6, pp.2329–2338.

Khan, I., Khan, S., Ahmed, H. and Nongjai, R. (2013) 'In structural and dielectric properties of Mn doped copper oxide (CuO) nanostructure', *AIP Conference Proceedings, American Institute of Physics*, pp.241–242.

Kikuchi, N. and Tonooka, K. (2005) 'Electrical and structural properties of Ni-doped Cu2O films prepared by pulsed laser deposition', *Thin Solid Films*, Vol. 486, Nos. 1–2, pp.33–37.

Kiriakidou, F., Kondarides, D.I. and Verykios, X.E. (1999) 'The effect of operational parameters and TiO2-doping on the photocatalytic degradation of azo-dyes', *Catalysis Today*, Vol. 54, No. 1, pp.119–130.

Mageshwari, K., Mali, S.S., Sathyamoorthy, R. and Patil, P.S. (2013) 'Template-free synthesis of MgO nanoparticles for effective photocatalytic applications', *Powder Technology*, Vol. 249, pp.456–462.

Marczenko, Z., Balcerzak, M. and Kuś, S. (1980) 'Spectrophotometric determination of ruthenium and osmium', *Talanta*, Vol. 27, No. 12, pp.1087–1089.

Masudy-Panah, S., Siavash Moakhar, R., Chua, C.S., Tan, H.R., Wong, T.I., Chi, D. and Dalapati, G.K. (2016) 'Nanocrystal engineering of sputter-grown CuO photocathode for visible-light-driven electrochemical water splitting', *ACS Applied Materials & Interfaces*, Vol. 8, No. 2, pp.1206–1213.

Meneses, C., Duque, J., Vivas, L. and Knobel, M. (2008) 'Synthesis and characterization of TM-doped CuO (TM = Fe, Ni)', *Journal of Non-Crystalline Solids*, Vol. 354, Nos. 42–44, pp.4830–4832.

Nandy, S., Maiti, U., Ghosh, C. and Chattopadhyay, K. (2009) 'Enhanced p-type conductivity and band gap narrowing in heavily Al doped NiO thin films deposited by RF magnetron sputtering', *Journal of Physics: Condensed Matter*, Vol. 21, No. 11, p.115804.

Ogwu, A., Darma, T. and Bouquerel, E. (2007) 'Electrical resistivity of copper oxide thin films prepared by reactive magnetron sputtering', *Journal of Achievements in Materials and Manufacturing Engineering*, Vol. 24, No. 1, pp.172–177.

Pollack, G. and Trivich, D. (1975) 'Photoelectric properties of cuprous oxide', *Journal of Applied Physics*, Vol. 46, No. 1, pp.163–172.

Prabu, R.D., Valanarasu, S., Kulandaisamy, I., Ganesh, V., Shkir, M. and Kathalingam, A. (2017) 'Studies on copper oxide thin films prepared by simple nebulizer spray technique', *Journal of Materials Science: Materials in Electronics*, Vol. 28, No. 9, pp.6754–6762.

Ramya, S., Viruthagiri, G., Gobi, R., Shanmugam, N. and Kannadasan, N. (2016) 'Synthesis and characterization of Ni 2+ ions incorporated CuO nanoparticles and its application in antibacterial activity', *Journal of Materials Science: Materials in Electronics*, Vol. 27, No. 3, pp.2701–2711.

Rao, G.N., Yao, Y. and Chen, J. (2007) 'Influence of Mn substitution on microstructure and magnetic properties of Cu_{1-x} Mn_x O nanoparticles', *Journal of Applied Physics*, Vol. 101, No. 9, p.09H119.

Shen, Y., Guo, M., Xia, X. and Shao, G. (2015) 'Role of materials chemistry on the electrical/electronic properties of CuO thin films', *Acta Materialia*, Vol. 85, pp.122–131.

Shkir, M. and AlFaify, S. (2017) 'Tailoring the structural, morphological, optical and dielectric properties of lead iodide through Nd 3+ doping', *Scientific Reports*, Vol. 7, No. 1, pp.1–9.

Sonia, S., Annsi, I.J., Kumar, P.S., Mangalaraj, D., Viswanathan, C. and Ponpandian, N. (2015) 'Hydrothermal synthesis of novel Zn doped CuO nanoflowers as an efficient photodegradation material for textile dyes', *Materials Letters*, Vol. 144, pp.127–130.

Tabuchi, N. and Matsumura, H. (2002) 'Control of carrier concentration in thin cuprous oxide Cu2O films by atomic hydrogen', *Japanese Journal of Applied Physics*, Vol. 41, No. 8R, p.5060.

Titirici, M-M., Antonietti, M. and Thomas, A. (2006) 'A generalized synthesis of metal oxide hollow spheres using a hydrothermal approach', *Chemistry of Materials*, Vol. 18, No. 16, pp.3808–3812.

Wang, Y., Jiang, T., Meng, D., Wang, D. and Yu, M. (2015) 'Synthesis and enhanced photocatalytic property of feather-like Cd-doped CuO nanostructures by hydrothermal method', *Applied Surface Science*, Vol. 355, pp.191–196.

Williamson, G. and Smallman III, R. (1956) 'Dislocation densities in some annealed and cold-worked metals from measurements on the X-ray debye-scherrer spectrum', *Philosophical Magazine*, Vol. 1, No. 1, pp.34–46.

Xu, M., Wang, F., Zhao, M., Yang, S., Sun, Z. and Song, X. (2011) 'Synthesis of copper oxide nanostructures via a composite-Hydroxide-mediated approach: morphology control and the electrochemical performances as anode material for lithium ion batteries', *Physica E: Low-dimensional Systems and Nanostructures*, Vol. 44, No. 2, pp.506–510.

Zhao, F., Qiu, H., Pan, L., Zhu, H., Zhang, Y., Guo, Z., Yin, J., Zhao, X. and Xiao, J.Q. (2008) 'Ferromagnetism analysis of Mn-doped CuO thin films', *Journal of Physics: Condensed Matter*, Vol. 20, No. 42, p.425208.